AEDC-TR-73-49

cy 2

A DESCRIPTION OF A FORCED-OSCILLATION TEST MECHANISM FOR MEASURING DYNAMIC-STABILITY DERIVATIVES IN ROLL

G. E. Burt

ARO, Inc.

June 1973

VON KÁRMÁN GAS DYNAMICS FACILITY
ARNOLD ENGINEERING DEVELOPMENT CENTER
AIR FORCE SYSTEMS COMMAND
ARNOLD AIR FORCE STATION, TENNESSEE

NOTICES

When U. S. Government drawings specifications, or other data are used for any purpose other than a definitely related Government procurement operation, the Government thereby incurs no responsibility nor any obligation whatsoever, and the fact that the Government may have formulated, furnished, or in any way supplied the said drawings, specifications, or other data, is not to be regarded by implication or otherwise, or in any manner licensing the holder or any other person or corporation, or conveying any rights or permission to manufacture, use, or sell any patented invention that may in any way be related thereto.

Qualified users may obtain copies of this report from the Defense Documentation Center.

References to named commercial products in this report are not to be considered in any sense as an endorsement of the product by the United States Air Force or the Government.

A DESCRIPTION OF A FORCED-OSCILLATION TEST MECHANISM FOR MEASURING DYNAMIC-STABILITY DERIVATIVES IN ROLL

G. E. Burt
ARO, Inc.

FOREWORD

The work reported herein was conducted by the Arnold Engineering Development Center (AEDC), Air Force Systems Command (AFSC), Arnold Air Force Station, Tennessee.

The results presented were obtained by ARO, Inc. (a subsidiary of Sverdrup & Parcel and Associates, Inc.), contract operator of AEDC. The apparatus was developed under ARO Project No. VA017, and the wind tunnel tests were conducted on May 9, 1972, under ARO Project No. VA206. The manuscript was submitted for publication on December 27, 1972.

This technical report has been reviewed and is approved.

JIMMY W. MULLINS
Lt Colonel, USAF
Chief Air Force Test Director, VKF
Directorate of Test

A. L. COAPMAN
Colonel, USAF
Director of Test

ABSTRACT

A description is given of a forced-oscillation, dynamic-stability test mechanism for measuring the moments and forces due to roll velocity on lifting configurations. The mechanism can support models with a combined loading of up to 1200 pounds of normal force and 300 pounds of axial force and is water-cooled to permit testing in hypersonic tunnels. Bench tests were conducted using a magnetic calibrator, which indicated that the mechanism could precisely measure the rolling moment, yawing moment, and side force due to roll velocity. Wind tunnel tests were conducted on an AGARD Model B at Mach numbers of 2, 3, and 4 and at angles of attack from -4 to 11 deg to verify the design. Results of these tests indicated good agreement between the experimental and theoretical values of the roll-damping coefficient, but the cross derivatives (yawing moment and side force) due to roll velocity could not be obtained for this particular model because of an adverse coupling of the roll and yaw natural frequencies and a large product of inertia of the model.

CONTENTS

		Page
	ABSTRACT	iii
	NOMENCLATURE	vi
I.	INTRODUCTION	1
II.	APPARATUS	
	2.1 Test Mechanism	1
	2.2 Instrumentation	4
	2.3 Model	5
	2.4 Wind Tunnel	10
III.	PROCEDURE	
	3.1 Data Reduction	10
	3.2 Calibration and Bench Tests	13
	3.3 Wind Tunnel Tests	13
IV.	PRECISION OF MEASUREMENTS	14
V.	RESULTS AND DISCUSSION	16
VI.	CONCLUSIONS	22
	REFERENCES	22

ILLUSTRATIONS

Figure

1. Test Mechanism
   a. Details . . . 2
   b. Photograph of the Flexures and Water Jacket . . 3
   c. Photograph of the Balance . . . 3
2. Instrumentation Console . . . 4
3. Data Acquisition Instrumentation Schematic
   a. Balance Outputs . . . 6
   b. Resolver System . . . 7
4. Model Description
   a. Details . . . 8
   b. Installation Photograph . . . 9

Figure Page

5. Comparison of Roll-Damping Measurement to Magnetic Calibrator Input
   a. Variation with Damping Magnitude 17
   b. Variation with Phase Angle and Frequency. . . . 17
6. Comparison of Measured Yawing Moment and Side Force due to Roll Velocity to Magnetic Calibrator Input
   a. Variation with Yawing Moment and Side Force Due to Roll Velocity. 18
   b. Variation with Frequency 18
7. Variation of Roll-Damping Coefficients with Angle of Attack and Mach Number. 20
8. Variation of Normal-Force and Pitching-Moment Coefficients with Angle of Attack and Mach Number. . . 21

TABLES

I. Summary of Test Conditions 13

II. Data Uncertainty. 16

NOMENCLATURE

A	Reference area, model wing area, 0.974 ft^2
b	Reference length for lateral coefficients, wing span, 1.500 ft
C_ℓ	Rolling-moment coefficient, $L/q_\infty Ab$
C_{ℓ_p}	Rolling-moment coefficient due to roll velocity $\partial(C_\ell)/\partial(pb/2V_\infty)$, $radian^{-1}$
C_{ℓ_β}	Rolling-moment coefficient due to sideslip angle, $\partial(C_\ell)/\partial\beta$, $radian^{-1}$
$C_{\ell_{\dot\beta}}$	Rolling-moment coefficient due to rate of change of sideslip angle, $\partial(C_\ell)/\partial(\dot\beta b/2V_\infty)$, $radian^{-1}$

C_m	Pitching-moment coefficient, $M/q_\infty Ac$
C_N	Normal-force coefficient, Normal Force$/q_\infty A$
C_n	Yawing-moment coefficient, $N/q_\infty Ab$
C_{n_p}	Yawing-moment coefficient due to roll rate, $\partial(C_n)/\partial(pb/2V_\infty)$, radian^{-1}
$C_{n_{\dot\beta}}$	Yawing-moment coefficient due to rate of change of sideslip angle, $\partial(C_n)/\partial(\dot\beta b/2V_\infty)$, radian^{-1}
C_Y	Side-force coefficient, $Y/q_\infty A$
$C_{Y_{\dot\beta}}$	Side-force coefficient due to rate of change of sideslip angle, $\partial(C_Y)/\partial(\dot\beta b/2V_\infty)$, radian^{-1}
C_{Y_p}	Side-force coefficient due to roll velocity, $\partial(C_Y)/\partial(pb/2V_\infty)$, radian^{-1}
c	Reference length for longitudinal coefficients, wing mean aerodynamic chord, 0.866 ft
I_x	Model moment of inertia about the x axis, slug-ft^2
I_{xz}	Product of inertia about the x and z axes, slug-ft^2
I_z	Model moment of inertia about the z axis, slug-ft^2
K_0	Flexure calibration constant, radians/volt
K_1, K_2	Balance forward and aft pitching-moment calibration constants, ft-lb/volt
K_3, K_4	Balance forward and aft yawing-moment calibration constants, ft-lb/volt
K_5	Balance rolling-moment calibration constant, ft-lb/volt
L	Moment about the model x axis (rolling moment), ft-lb
L_b	Input torque in roll, ft-lb
L_β	Rolling moment due to sideslip angle, $\partial L/\partial\beta$, ft-lb/radian
$L_{\dot\beta}$	Rolling moment due to rate of change of sideslip angle, $\partial L/\partial\dot\beta$, ft-lb-sec/radian
L_ϕ	Rolling moment due to roll angle, $\partial L/\partial\phi$, ft-lb/radian
$L_{\dot\phi}$	Rolling moment due to rate of change of roll angle, $\partial L/\partial\dot\phi$, ft-lb-sec/radian

M	Moment about the model y axis (pitching-moment), ft-lb
M_∞	Free-stream Mach number
N	Moment about the model z axis (yawing-moment), ft-lb
N_β	Yawing moment due to sideslip angle, $\partial N/\partial\beta$, ft-lb/radian
$N_{\dot\beta}$	Yawing moment due to rate of change of sideslip angle, $\partial N/\partial\dot\beta$
$N_{\dot\phi}$	Yawing moment due to rate of change of roll angle, $\partial N/\partial\dot\phi$, ft-lb-sec/radian
N_ψ	Yawing moment due to yaw angle, $\partial N/\partial\psi$, ft-lb/radian
$N_{\dot\psi}$	Yawing moment due to rate of change of yaw angle, $\partial N/\partial\dot\psi$, ft-lb-sec/radian
p	Rolling velocity, radians/sec
p_o	Tunnel stilling chamber pressure, psia
q_∞	Tunnel free-stream dynamic pressure, lb/ft^2
$Re_{\infty, c}$	Tunnel free-stream Reynolds number based on c
T_o	Tunnel stilling chamber temperature, °R
t	Time, sec
V_∞	Tunnel free-stream velocity, ft/sec
x, y, z	Body-fixed axis system
x_1, x_2	Location of forward and aft yaw strain gage electrical centers, respectively, ft
x_R	Location of moment reference point, ft
Y	Side force, lb
$Y_{\dot\beta}$	Side force due to rate of change of sideslip angle, $\partial Y/\partial\dot\beta$, lb-sec/radian
$Y_{\dot\phi}$	Side force due to rate of change of roll angle, $\partial Y/\partial\dot\phi$, lb-sec/radian
α	Angle of attack, deg
β	Sideslip angle, radians
Γ	Phase angle between yawing moment, N, and roll angle, ϕ (positive when N leads), radians

γ	Phase angle between input torque, L_b, and roll angle, ϕ (positive when L_b leads), radians or deg
ϕ	Angular displacement about the x axis (roll angle), radians or deg
ψ	Angular displacement about the z axis (yaw angle), radians
ω	Model angular oscillation frequency, radians/sec
ω_{n_ϕ}	Model-flexure natural frequency in roll at vacuum conditions, radians/sec
ω_{n_ψ}	Model-flexure natural frequency in yaw at vacuum conditions, radians/sec
$(\dot{})(\ddot{})$	First and second derivatives with respect to time, t
$(\bar{})$	Amplitude
$\Delta( )$	Probable error

SUBSCRIPTS

a	Aerodynamic
b	Balance
f	Flexure
mag	Magnetic calibrator
r	Resolvers
S	Static
1	Forward balance section
2	Aft balance section

SECTION I
INTRODUCTION

The advent of high performance, supersonic military airplanes and reentry lifting bodies such as the F-15, the B-1, and the Space Shuttle has created the requirement to develop new dynamic-stability test mechanisms for the von Kármán Gas Dynamics Facility (VKF) continuous-flow wind tunnels. To meet the requirements for large lift loads and relatively large damping moments, and to maintain compatibility with expected model configurations, the forced-oscillation technique has been selected. This is a proven technique currently being used at VKF for measuring damping coefficients due to pitch and yaw rate on configurations with relatively low lift forces (Ref. 1). This report covers the development and checkout, including wind tunnel verification testing, of a mechanism used to determine the coefficients due to roll rate (rolling moment, yawing moment, and side force) on lifting configurations. This mechanism can support models with a combined loading of up to 1200 lb of normal force and 300 lb of axial force. Although this mechanism was designed primarily to obtain dynamic measurements, the technique employed also produces five-component static force and moment data. The mechanism was primarily intended for use in the VKF supersonic and hypersonic wind tunnels (Mach 1.5 to 12), but it can be used in the Propulsion Wind Tunnel Facility (PWT) transonic and supersonic tunnels (Mach 0.2 to 4.75).

The wind tunnel verification tests were conducted in the VKF Supersonic Wind Tunnel (A) at Mach numbers 2, 3, and 4 on an AGARD Calibration Model B. A test mechanism to measure the pitch and yaw stability derivatives on high-load configurations has also been developed, and the results are reported in Ref. 2.

SECTION II
APPARATUS

2.1 TEST MECHANISM

The VKF 1.D roll-damping test mechanism (Fig. 1) utilizes a water-jacketed, five-component balance, twin beam flexures, roller bearings to support the loads, and electric printed-circuit drive motors. The motors are directly coupled to the balance and supply up to 120 in.-lb roll moment

to oscillate the system at amplitudes up to ±3 deg and at frequencies from 2 to 20 Hz. The twin beam flexures mount from the stationary sting to the oscillating water jacket and provide a restoring moment which cancels the inertia moment when the system is operating at the natural frequency of the model-flexure system. The flexures are instrumented to measure the roll displacement. The entire mechanism is water-cooled to permit testing in the hypersonic tunnels.

Two five-component balances have been fabricated for the system to provide good balance sensitivity over the load range. Both balances utilize outrigger beams in the yaw sections (Fig. 1c) and thin-ribbed flexures in the roll section to provide sensitive yaw and roll outputs while maintaining large normal-force capacity and rigidity in yaw. Semiconductor gages are also utilized for the yaw and roll sections for additional sensitivity. The load capacity of the two balances is listed below:

Balance	Normal Force	Pitching Moment	Side Force	Yawing Moment	Rolling Moment
-59	500 lb	1125 in.-lb	40 lb	84 in.-lb	10 in.-lb
-60	1200 lb	2700 in.-lb	100 lb	210 in.-lb	100 in.-lb

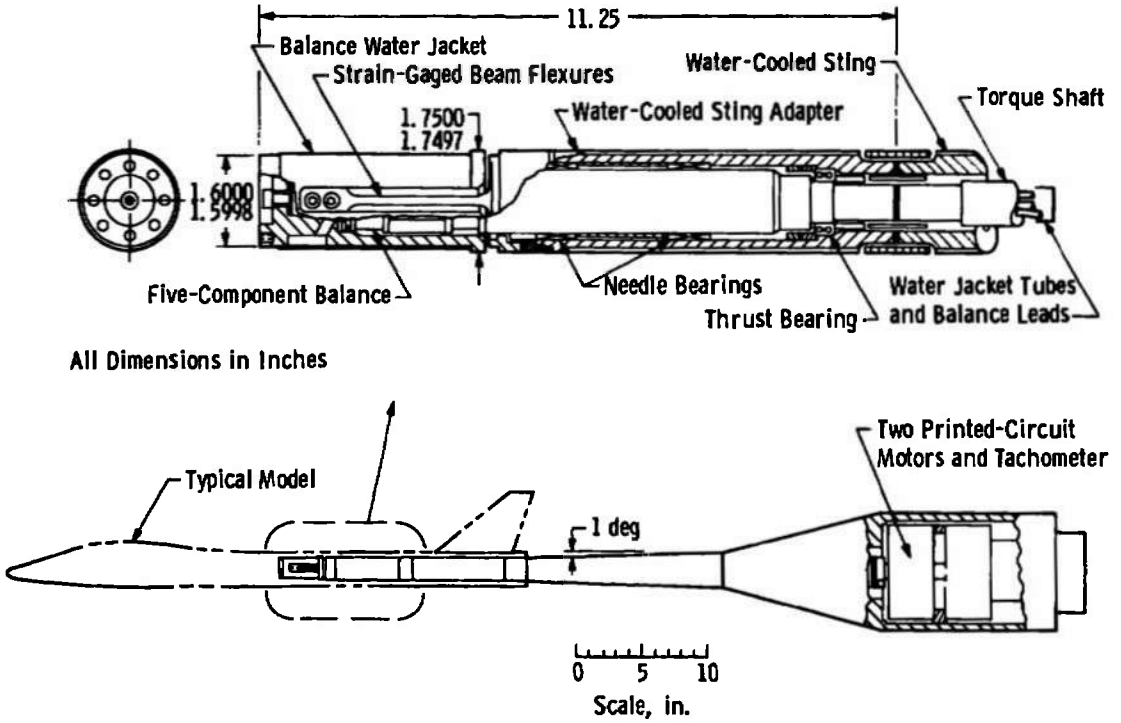

a. Details

Fig. 1 Test Mechanism

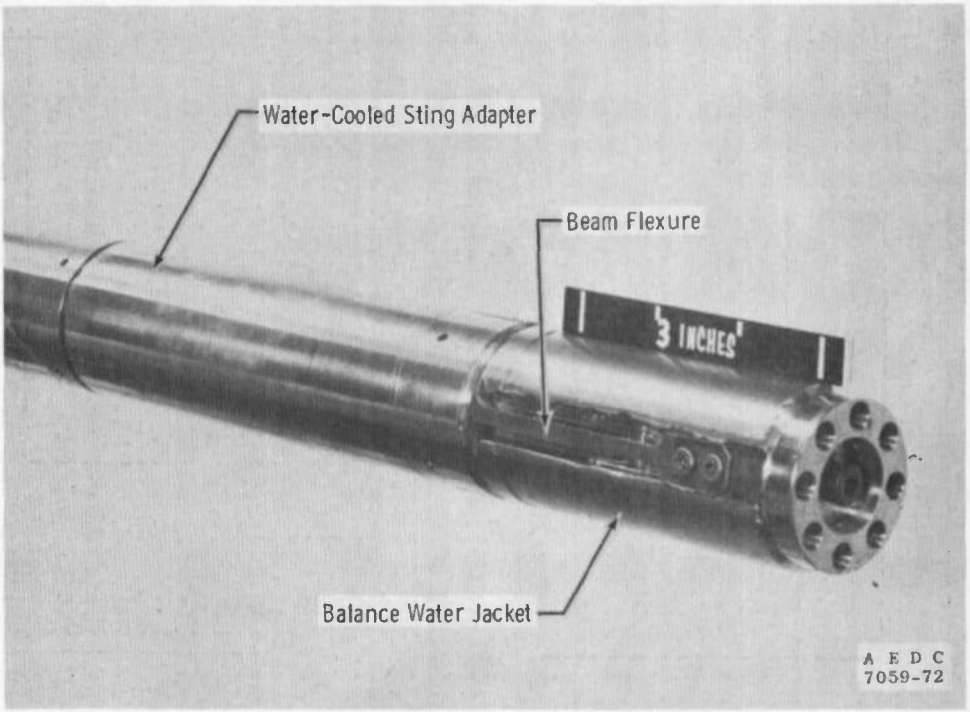

b. Photograph of the Flexures and Water Jacket

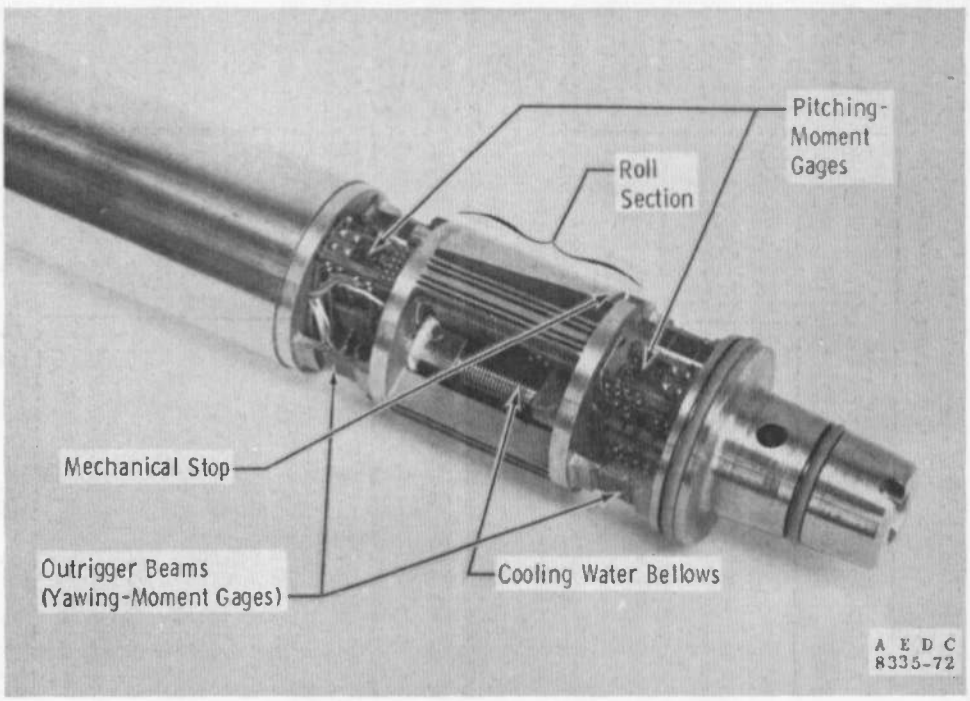

c. Photograph of the Balance
Fig. 1 Concluded

2.2 INSTRUMENTATION

The forced-oscillation instrumentation described in Ref. 1 was modified to improve the control and monitor systems and thereby to provide more accurate data with less computer time required. These changes were made by using an electronic analog system with precision electronics. The control, monitor, and data acquisition instrumentation is contained in a portable console (Fig. 2) that can be easily interfaced with the instrumentation of the various wind tunnels.

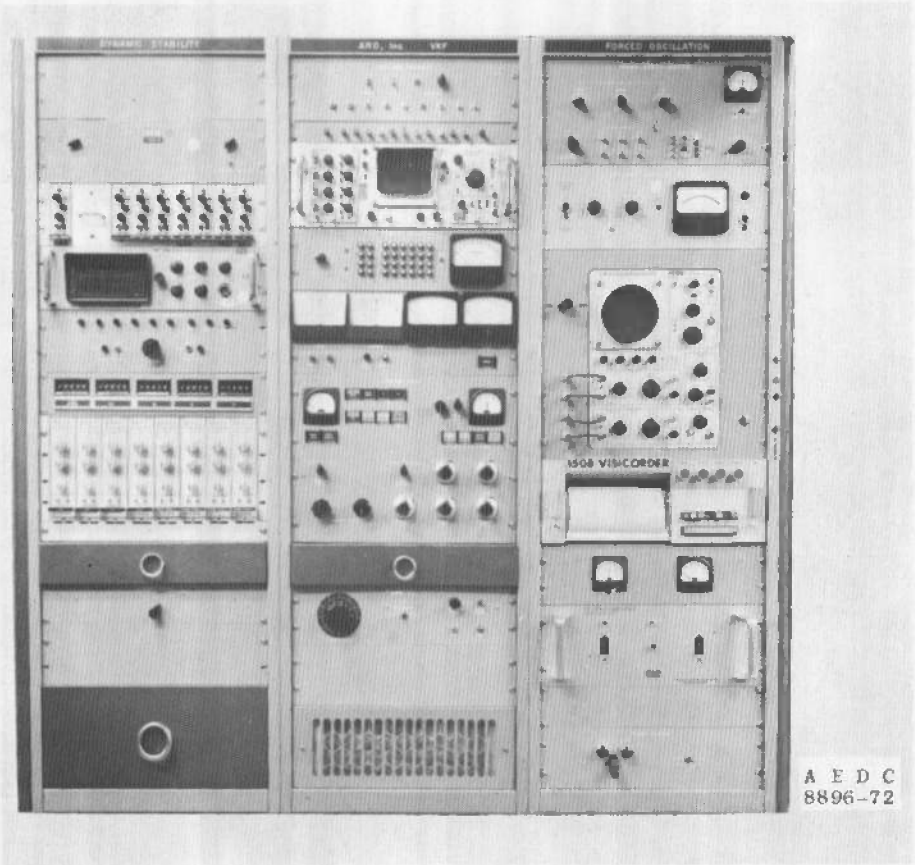

Fig. 2 Instrumentation Console

The control instrumentation provides a system which can vary the oscillation frequency, oscillation amplitude, and roll position of the model within the flexure limits. The oscillation amplitude is controlled by an electronic feedback loop which permits testing both dynamically stable and unstable configurations.

Data are normally obtained at or near the natural frequency of the model-flexure system; however, the electronic resolvers used permit data to be obtained off resonance. A schematic of the data acquisition system is shown in Fig. 3. The gages on the balance and flexures are excited by d-c voltages, and outputs are increased to optimum values by d-c amplifiers. Typical balance and flexure outputs from an oscillating model are composed of oscillatory components (OC) superimposed on static components (SC). These components are separated in the data system by bandpass and lowpass filters. The SC outputs are sent directly to the tunnel scanner and computer, which calculate the static-force and moment coefficients, C_N, C_m, C_Y, C_n, and C_ℓ. The OC outputs are input to the resolver instrumentation (Fig. 3b) and the precise frequency-measuring instrument which were developed at VKF. The resolvers utilize very accurate analog electronic devices to process the OC signals and output d-c voltages, which are proportional to the amplitude squared, the in-phase and quadrature (90 deg out of phase) rolling moments, and the quadrature yawing moments. A switch is also provided in the resolver system to bypass the phase shift network so that the in-phase yawing moments can be determined. The resolver and frequency outputs are read by the tunnel scanner and sent to the computer. The frequency instrument controls the length of the data interval in increments from approximately 2 to 25 seconds, during which time the scanner reads each input approximately 10 times per second. The average values of the readings are calculated by the computer, which then uses these average values to calculate the dynamic coefficients $C_{\ell_p} + C_{\ell_{\dot\beta}} \sin\alpha$, $C_{n_p} + C_{n_{\dot\beta}} \sin\alpha$, and $C_{Y_p} + C_{Y_{\dot\beta}} \sin\alpha$ as described in Section 3.1.

2.3 MODEL

The model used for the wind tunnel verification testing was a 4.5-in.-diam AGARD Calibration Model B (Fig. 4) which was obtained on loan from the Cornell Aeronautical Laboratory. The body is a tangent ogive cylinder with a fineness ratio of 8.5. The 60-deg delta wing has a symmetrical, circular-arc cross section with a thickness ratio of 0.04 and a span of four body diameters. The model was constructed primarily of aluminum but contained some steel for additional strength at the wing mounting location. The model was mounted to the test mechanism in such a way that there was a distance of nearly 4.5 body diameters from the model base to the sting flare.

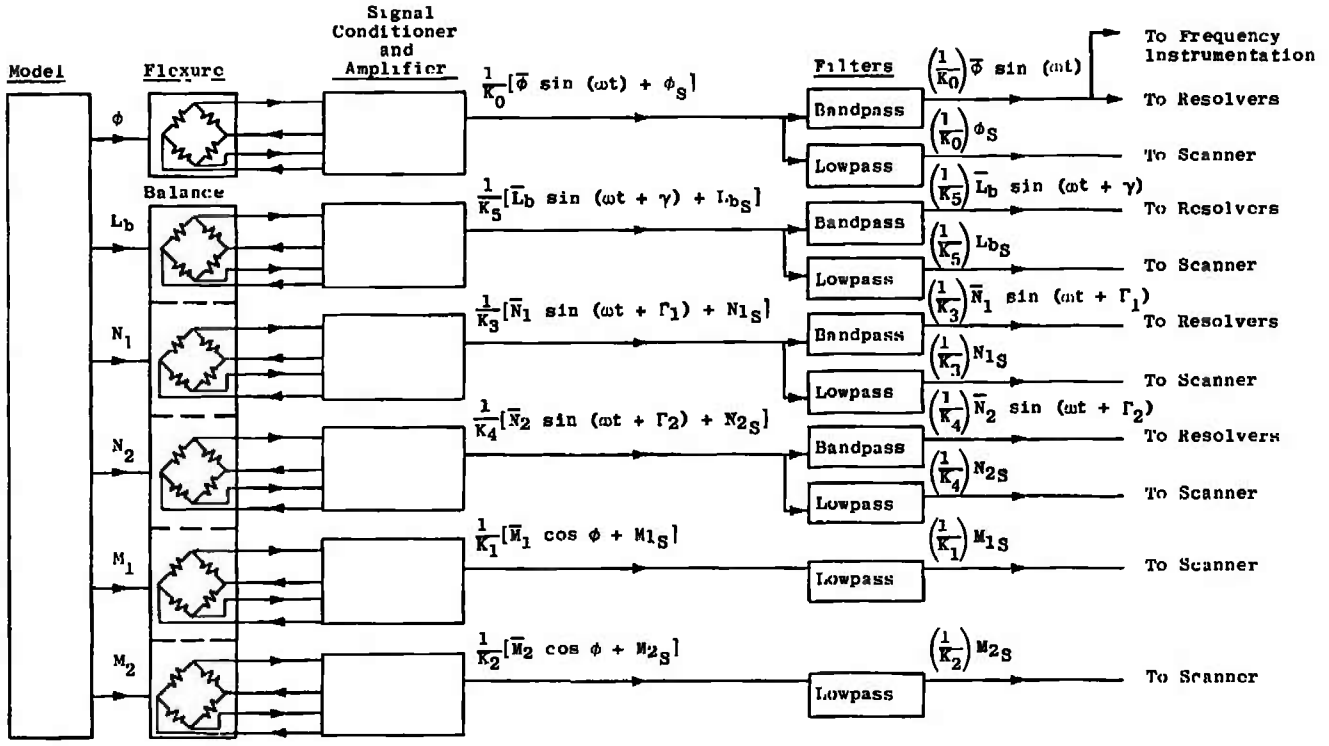

a. Balance Outputs

Fig. 3 Data Acquisition Instrumentation Schematic

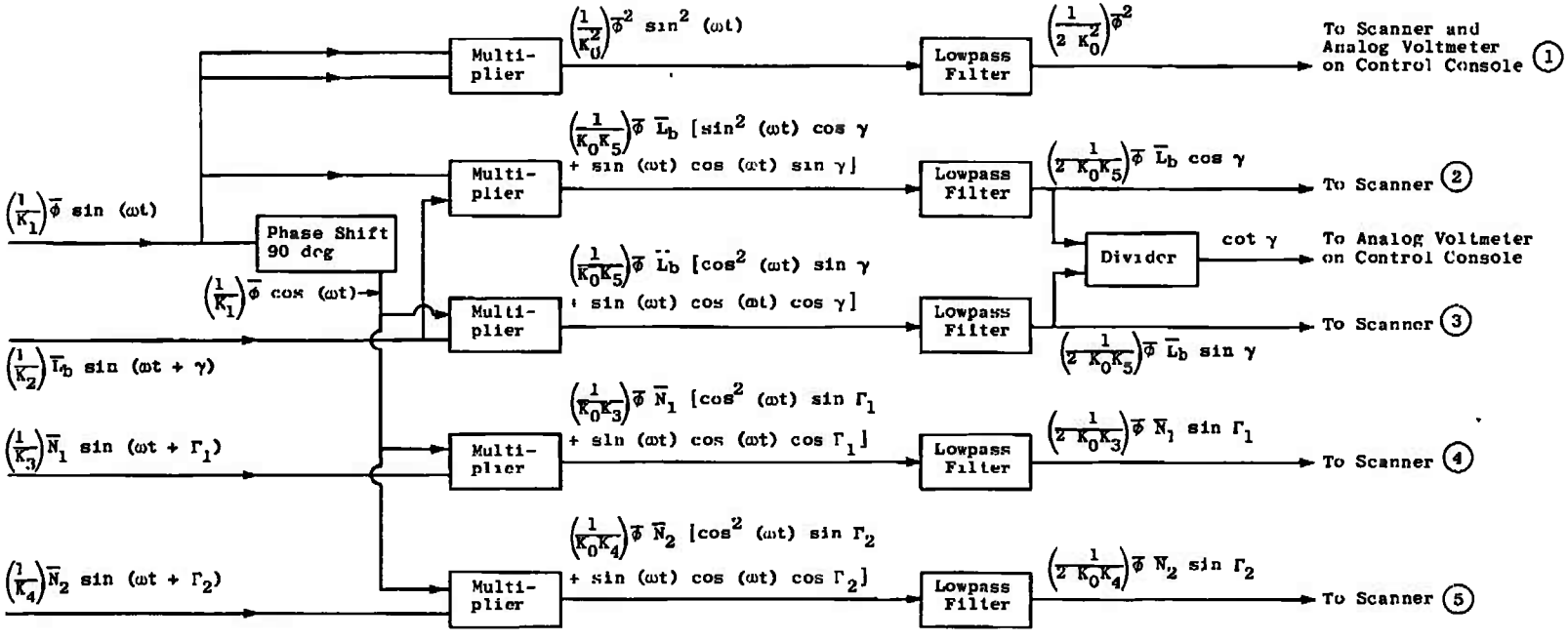

b. Resolver System

Fig. 3 Concluded

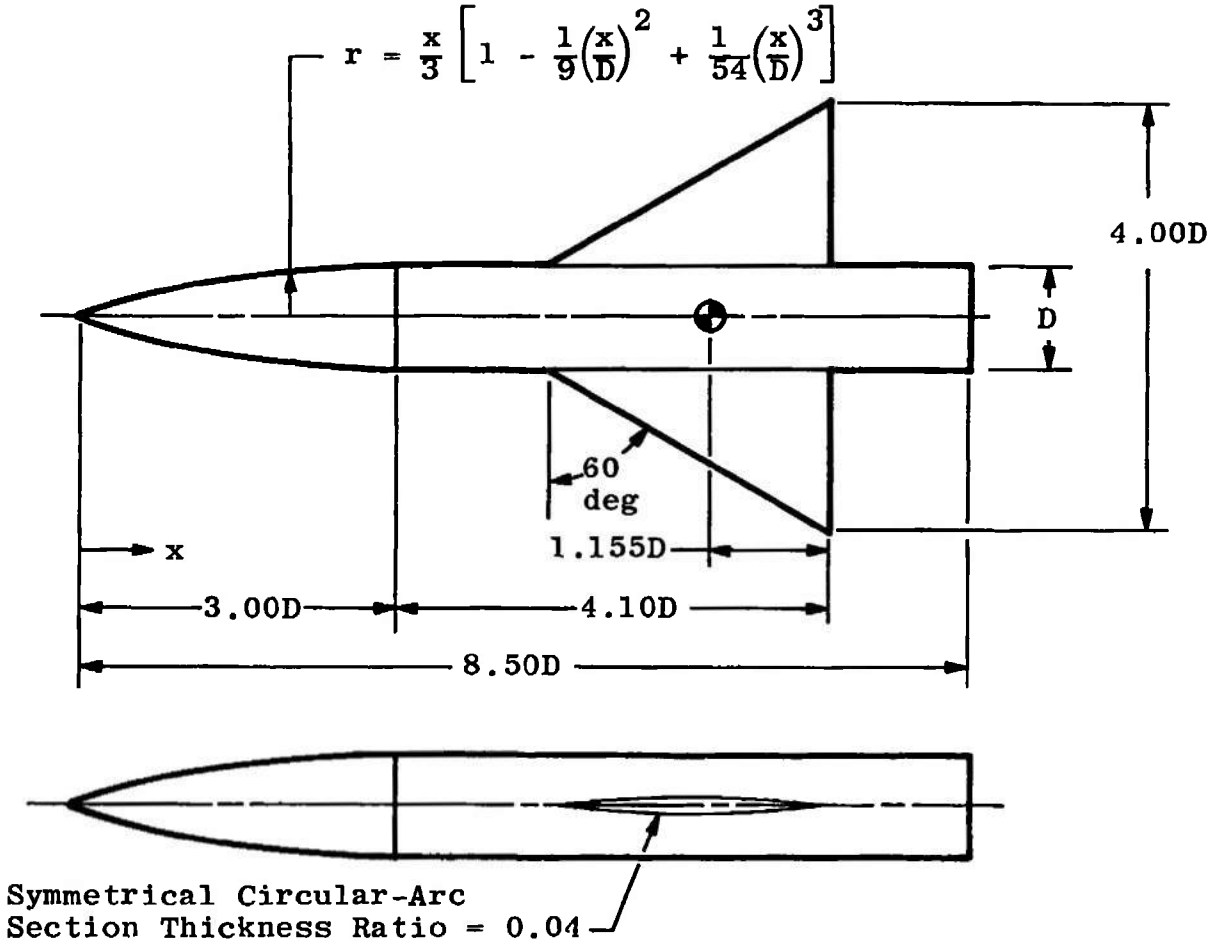

All Dimensions in Body Diameters, D (D = 4.50 in.)

◓ Indicates Moment Reference Point

a. Details

Fig. 4 Model Description

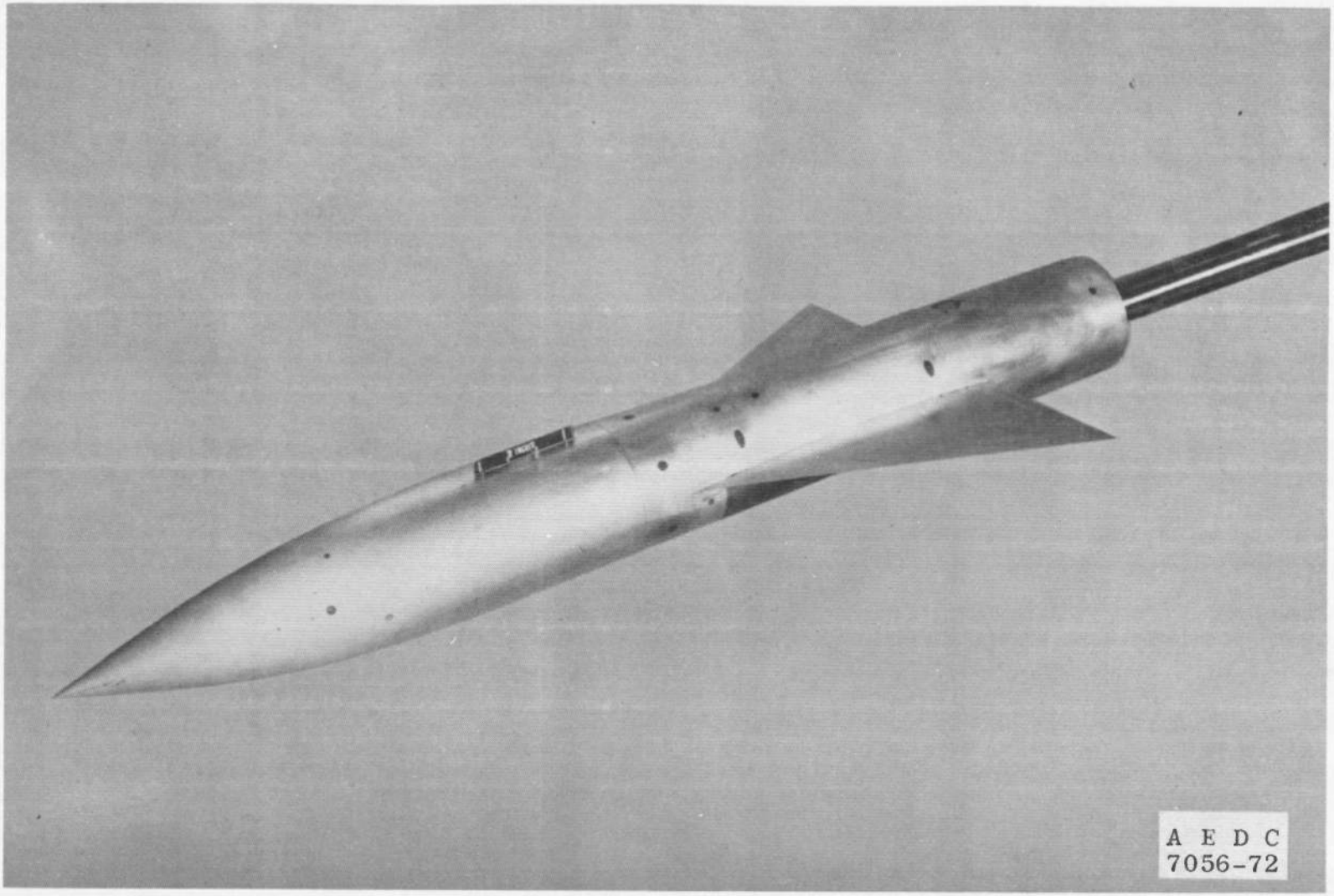

b. Installation Photograph
Fig. 4 Concluded

2.4 WIND TUNNEL

Tunnel A is a continuous, closed-circuit, variable density wind tunnel with an automatically driven flexible-plate-type nozzle and a 40- by 40-in. test section. The tunnel can be operated at Mach numbers from 1.5 to 6 at maximum stagnation pressures from 29 to 200 psia, respectively, and stagnation temperatures up to 750°R (at $M_\infty = 6$). Minimum operating pressures range from about one-tenth to one-twentieth of the maximum pressure at each Mach number. In most instances, Mach number changes may be made without stopping the tunnel. The model can be injected into the tunnel for a test run and then retracted for model changes without stopping the tunnel flow.

SECTION III
PROCEDURE

3.1 DATA REDUCTION

The test mechanism operates basically as a one-degree-of-freedom system in roll (body axis system); however, it is obvious that for the balance to measure the dynamic yawing moments it must also deflect in yaw. Therefore, both the roll and yaw equations of motion must be considered. These equations can be simplified considerably if the balance is made very stiff in the yaw direction and the system is not operated near the natural yaw frequency ($\omega_{n_\psi} > 1.5\omega$). With these conditions it is assumed that

$$\sin\phi = \phi$$
$$\psi \ll \phi$$
$$N_{\psi b} \gg N_{\psi a}$$
$$N_{\dot{\psi}}\,\dot{\psi} = 0$$

Now the roll equation of motion can be written

$$I_x\ddot{\phi} - \left(L_{\dot{\phi}_a} + L_{\dot{\beta}_a}\sin\alpha + L_{\dot{\phi}_f}\right)\dot{\phi} - \left(L_{\beta_a}\sin\alpha + L_{\phi_f}\right)\phi = L_b \qquad (1)$$

which is independent of yaw. The yaw equation of motion can be written

$$I_z\ddot{\psi} + I_{xz}\ddot{\phi} - \left(N_{\dot{\phi}} + N_{\dot{\beta}}\sin\alpha + N_{\dot{\phi}_f}\right)\dot{\phi} - N_\beta\sin\alpha\,\phi = N_{\psi_b}\psi \qquad (2)$$

The solution of these equations for a system oscillating at a steady-state condition at some amplitude, $\bar{\phi}$, may be written

$$\begin{aligned} \phi &= \bar{\phi} \cos \omega t \\ L_b &= \bar{L}_b \cos (\omega t - \gamma) \\ \psi &= \bar{\psi} \cos (\omega t + \Gamma) \end{aligned} \tag{3}$$

Now substituting in the roll equation gives

$$\left(L_{\dot{\phi}} + L_{\dot{\beta}} \sin \alpha\right)_a = \left(-\frac{\bar{L}_b}{\bar{\phi}} \sin \gamma - L_{\dot{\phi}_f} \omega\right) \frac{1}{\omega} \tag{4}$$

and

$$\left(L_\beta \sin \alpha\right)_a = -\frac{\bar{L}_b}{\bar{\phi}} \cos \gamma + L_{\phi_f} \left[\left(\frac{\omega}{\omega_{n_\phi}}\right)^2 - 1\right] \tag{5}$$

where $-L_{\phi_f}/(\omega_{n_\phi})^2$ has been substituted for I_x. The terms $(\bar{L}_b/\bar{\phi}) \sin \gamma$ and $(\bar{L}_b/\bar{\phi}) \cos \gamma$ can be obtained directly from the resolvers (Fig. 3b) by dividing outputs 3 and 2, respectively, by output 1 and the appropriate balance calibration factors. L_{ϕ_f} is determined in the flexure-balance calibration, and $L_{\dot{\phi}_f}$ and ω_{n_ϕ} can be obtained by evaluating the system at vacuum conditions in a manner similar to that discussed for pitch in Ref. 1. The damping of the beam flexure, $L_{\dot{\phi}_f}$, varies inversely with frequency (i.e., $L_{\dot{\phi}_f}\omega$ is constant), which is the same result found for cross flexures in Ref. 3.

Now substituting Eqs. (3) in the yaw equation of motion (Eq. 2) and taking the quadrature (i.e., sin ωt) terms gives

$$\left(N_{\dot{\phi}} + N_{\dot{\beta}} \sin \alpha\right)_n = -\frac{\bar{\psi} \sin \Gamma}{\bar{\phi}\, \omega} \left[N_{\psi_b} + I_z(\omega)^2\right] - N_{\dot{\phi}_f} \tag{6}$$

Now substituting $-N_{\psi_b}/(\omega_{n_\psi})^2$ for I_z and realizing $N_{\psi_b}\, \psi$ is the moment measured by the balance, N, Eq. (6) can be written

$$\left(N_{\dot{\phi}} + N_{\dot{\beta}} \sin \alpha\right)_{a_{1,2}} = -\frac{\bar{N}_{1,2} \sin \Gamma}{\bar{\phi}\, \omega} \left[1 - \left(\frac{\omega}{\omega_{n_\psi}}\right)^2\right] - N_{\dot{\phi}_f} \tag{7}$$

where 1 and 2 denote moments obtained from forward and aft yaw sections of the balance, respectively. The terms $\overline{N}_{1,2} \sin \overline{\Gamma}/\overline{\phi}$ are obtained from resolver outputs 4, 5, and 1 (Fig. 3b), ω_{n_ψ} can be obtained by wind-off, free oscillation, and $N_{\dot{\phi}_f}$ can be obtained by evaluating the system at vacuum. The side force due to roll rate can be determined from the two yawing moments obtained from Eq. (7) as

$$\left(Y_{\dot{\phi}} + Y_{\dot{\beta}} \sin \alpha\right)_a = \frac{\left(N_{\dot{\phi}} + N_{\dot{\beta}} \sin \alpha\right)_{a_2} - \left(N_{\dot{\phi}} + N_{\dot{\beta}} \sin \alpha\right)_{a_1}}{x_1 - x_2} \tag{8}$$

It should be noted that although the in-phase terms of the yaw equation were not required to obtain the desired data, they can be important in two respects. First, if the product of inertia term $I_{xz} \ddot{\phi}$ is large, it produces a large yaw-forcing function which increases the yaw amplitude in such a way that the balance capacity is reached or the assumption that $\psi << \phi$ may be invalidated. Second, a portion of the in-phase terms is inherently included in the out-of-phase measurement because of resolver uncertainty, and thus it is desirable to minimize the in-phase term in order to get better data precision.

The parameters obtained in Eqs. (4), (5), (7), and (8) can be expressed in coefficient form as follows:

$$C_{\ell_p} + C_{\ell_{\dot{\beta}}} \sin \alpha = \frac{\left(L_{\dot{\phi}} + L_{\dot{\beta}} \sin \alpha\right)_a \left(2V_\infty\right)}{q_\infty A b^2}$$

$$C_{\ell_\beta} \sin \alpha = \frac{\left(L_\beta \sin \alpha\right)_a}{q_\infty A b}$$

$$C_{n_p} + C_{n_{\dot{\beta}}} \sin \alpha = \frac{\left[\left(N_{\dot{\phi}} + N_{\dot{\beta}} \sin \alpha\right)_{a_1} \left(x_R - x_2\right) - \left(N_{\dot{\phi}} + N_{\dot{\beta}} \sin \alpha\right)_{a_2} \left(x_R - x_1\right)\right] 2V_\infty}{\left(x_1 - x_2\right) q_\infty A b^2}$$

$$C_{Y_p} + C_{Y_{\dot{\beta}}} \sin \alpha = \frac{\left(Y_{\dot{\phi}} + Y_{\dot{\beta}} \sin \alpha\right)_a \left(2V_\infty\right)}{q_\infty A b}$$

In the preceding analysis the balance input torque, L_b, and yawing moment, N, signals have been assumed to be the first harmonic of the oscillation frequency, ω. Because of nonlinear aerodynamics, tunnel noise, flow perturbations, etc., these signals are often composed of higher and lower harmonics. However, the resolver system

(Fig. 3b) eliminates the higher harmonics, and the lower harmonics can be eliminated by averaging the data over a sufficiently long interval.

3.2 CALIBRATION AND BENCH TESTS

A complex balance calibration was required, which involved calibration of the balance and flexures separately and then in combination to determine all the calibration constants and interaction terms. For the present balances, the interactions affecting the dynamic measurements were small and usually negligible.

Bench tests were conducted with the system to determine its capability in measuring the dynamic quantities. A VKF-developed two-arm magnetic calibrator was used to produce known moments and forces proportional to roll velocity. A signal coil, input coil, and feedback loop were used in such a way that both stable and unstable roll moments could be produced by changing the phasing of the input coil on both arms. By changing the phasing of the input coil on one arm only, a side force and yawing moment proportional to the roll velocity could be created. The magnitude of these forces and moments could be varied by changing the gain in the feedback loop.

3.3 WIND TUNNEL TESTS

Tests were conducted on a 4.50-in.-diam AGARD Model B at Mach numbers 2, 3, and 4, at Reynolds numbers 0.76, 4.08, and 5.38 million, and at angles of attack from -4 to 11 deg. The data were obtained primarily at an oscillation amplitude, $\bar{\phi}$, of 1.2 deg and near the roll resonant frequency (i.e., $\gamma \approx 90$ deg); however, some data were obtained off resonance ($20 < \gamma < 160$) to check the resolvers. Wind-off data were obtained several times during the test to evaluate the flexure damping, $L_{\dot{\phi}_f}$, and roll natural frequency, ω_{n_ϕ}. A summary of the test conditions is presented in Table I.

TABLE I
SUMMARY OF TEST CONDITIONS

Mach No.	p_o, psia	T_o, °R	q_∞, lb/ft^2	V_∞, ft/sec	$Re_{\infty, c} \times 10^{-6}$	α, deg
2.00	19	562	979	1732	3.99	-4.5 to 10.3
3.01	32	562	784	2086	4.05	-4.4 to 11.0
3.99	10	562	107	2267	0.76	-4.3 to 10.9
4.02	55	562	575	2271	4.10	-4.3 to 10.7
4.03	72	562	746	2272	5.34	-4.1 to 10.1

SECTION IV
PRECISION OF MEASUREMENTS

The uncertainty in the measurements is a function of the precision of the calibration constants, instrumentation accuracy, repeatability of the flexure characteristics (wind-off data), and the frequency and phase relations. The uncertainties in the dynamic data as a result of the propagation of these errors (Ref. 4) can be written as follows:

$$\frac{\Delta\left(L_{\dot\phi}\dot\phi + L_{\dot\beta}\dot\beta \sin\alpha\right)}{\left(L_{\dot\phi}\dot\phi + L_{\dot\beta}\dot\beta \sin\alpha\right)} = \sqrt{\left(2.00 \times 10^{-4}\right) + \left[\frac{\Delta L_{\dot\phi_f}\dot\phi}{\left(L_{\dot\phi}\dot\phi + L_{\dot\beta}\dot\beta \sin\alpha\right)}\right]^2 + \left(\frac{\Delta\gamma_r}{\tan\gamma}\right)^2}$$

$$\frac{\Delta\left(L_\beta \sin\alpha\right)}{L_\beta \sin\alpha} = \sqrt{\left(2.50 \times 10^{-5}\right) + 1\left[\left(\frac{\Delta\omega_{n_\phi}}{\omega_{n_\phi}}\right)\left(\frac{L_{\phi_f}}{L_\beta \sin\alpha}\right)\right]^2}$$

$$\frac{\Delta\left(N_{\dot\phi}\dot\phi + N_{\dot\beta}\dot\beta \sin\alpha\right)}{\left(N_{\dot\phi}\dot\phi + N_{\dot\beta}\dot\beta \sin\alpha\right)} = \sqrt{\left(2.00 \times 10^{-4}\right) + \left[\frac{\Delta N_{\dot\phi_f}\dot\phi}{\left(N_{\dot\phi}\dot\phi + N_{\dot\beta}\dot\beta \sin\alpha\right)}\right]^2}$$

$$+ \left[\frac{1}{\tan\Gamma}\left(\Delta\Gamma_r + \frac{N_{\dot\psi}\dot\omega}{N_{\psi_h}}\right)\right]^2 + 10^{-1}\left[\left(\frac{\omega_{n_\psi}}{\omega}\right)^2 - 1\right]^{-2}$$

The uncertainty of the calibration constants (0.5 percent) and instrumentation uncertainties are combined in the first terms of the above equations. The second terms are uncertainties in the flexure characteristics. The third and fourth terms are uncertainties attributable to phase relations and assumptions. The resolver uncertainty is approximately 0.5 deg ($\Delta\gamma_r = \Delta\Gamma_r = 0.0087$ radians), but during the bench tests the system could easily be adjusted to maintain uncertainties within 0.25 deg.

It is apparent that the most accurate roll-damping data ($L_{\dot\phi}\dot\phi + L_{\dot\beta}\dot\beta \sin\alpha$) are obtained at the resonant frequency ($\gamma = 90$ deg), but the precision is not affected significantly if $30 < \gamma < 150$. The uncertainty

in the cross derivative ($N_{\dot{\phi}} + N_{\dot{\beta}} \sin \alpha$) can be drastically affected by the phase and frequency relationships. As stated previously, the oscillation frequency, ω, must not be near the natural yaw frequency, and the in-phase yawing moment needs to be minimized (i.e., as the in-phase moment increases, Γ approaches zero) to obtain good data. The yaw-damping term, $N_{\dot{\psi}}\dot{\psi}$, which was omitted in the data reduction equations, is small but may cause an error in the phase relation $N_{\dot{\psi}}\omega/N_{\psi_b}$ of the same magnitude as $\Delta\Gamma_r$.

Measurement of the tunnel model-support system pitch attitude is precise within 0.05 deg, based on repeat calibrations. Model attitude corrections were made for balance and sting deflections under air load, and the precision of the final model angle of attack, α, is estimated to be ±0.07 deg. The uncertainty in the static balance loads is determined from a statical analysis of the data obtained during calibration, where loads were applied in each plane and in combination, simulating the range of model loads anticipated for the test.

The preceding uncertainties were combined with uncertainties in the tunnel parameters and expanded using the Taylor series method of error propagation to obtain the probable error in the aerodynamic coefficients. The model used for these tests had a very large I_z to I_x ratio, and the natural yaw and roll frequencies were approximately equal. The model also had a fairly large product of inertia, I_{xz}, because of an unsymmetrical mounting section. Balast was added to the model to increase I_z in order to separate the natural frequencies ($\omega_{n_\phi} \approx 1.4\ \omega_{n_\psi}$), thus permitting the system to obtain roll-damping data; but, because of the large I_{xz} and adverse frequency coupling, the cross-derivative data could not be obtained. The uncertainties in all the parameters are presented in Table II.

TABLE II
DATA UNCERTAINTY

Parameter ()	Uncertainty			
	Bench Tests		Tunnel Tests	
	Δ()/() at () = max, %	Δ() at () = 0	Δ()/() at () = max, %	Δ() at () = 0
$L_{\dot{\phi}}^{\cdot} + L_{\dot{\beta}}^{\cdot} \sin \alpha$	1.4 at γ = 90 5.2 at γ = 5	0.00008	1.4	0.00020
$L_{\beta} \sin \alpha$	---	---	2.9	0.25
$N_{\dot{\phi}}^{\cdot} + N_{\dot{\beta}}^{\cdot} \sin \alpha$	2.0	0.00005	---	---
$Y_{\dot{\phi}}^{\cdot} + Y_{\dot{\beta}}^{\cdot} \sin \alpha$	2.8	0.00043	---	---
$C_{\ell_p} + C_{\ell_{\dot{\beta}}}^{\cdot} \sin \alpha$	---	---	1.8	0.0017
$C_{\ell_{\beta}} \sin \alpha$	---	---	3.1	0.00052
C_N	---	---	1.31	0.0028
C_m	---	---	1.02	0.00028

SECTION V
RESULTS AND DISCUSSION

The results obtained in the bench tests are presented in Figs. 5 and 6. The roll-damping measurement shows excellent agreement between the measured value and the calibrator input value over a large range of damping (Fig. 5a). The uncertainty in the calibrator is 2 percent of the input value, which is approximately the same uncertainty which Table II gives for the system. At the lower magnitudes the uncertainty of the flexure characteristics becomes the dominant factor. Figure 5b indicates that the resolvers can produce satisfactory results even when the system is operating far off resonance.

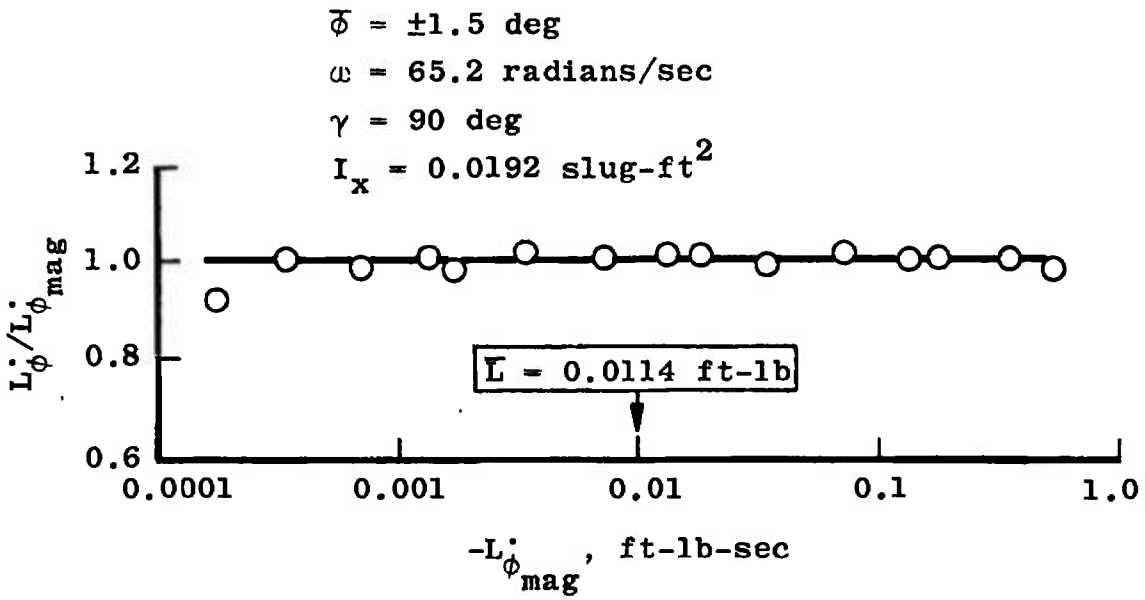

a. Variation with Damping Magnitude

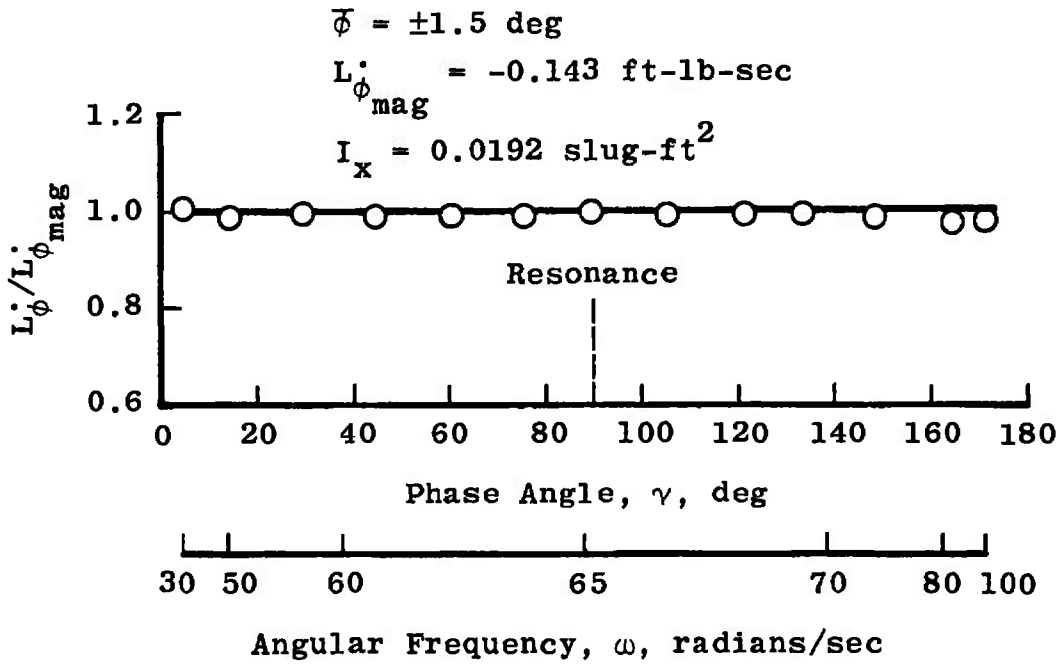

b. Variation with Phase Angle and Frequency

Fig. 5 Comparison of Roll-Damping Measurement to Magnetic Calibrator Input

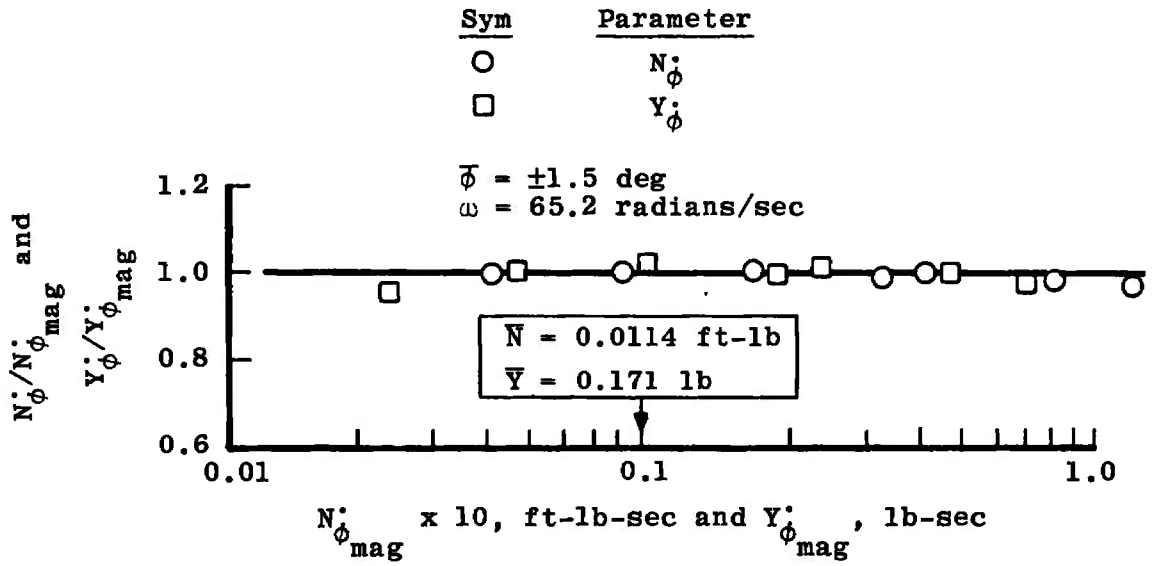

a. Variation with Yawing Moment and Side Force due to Roll Velocity

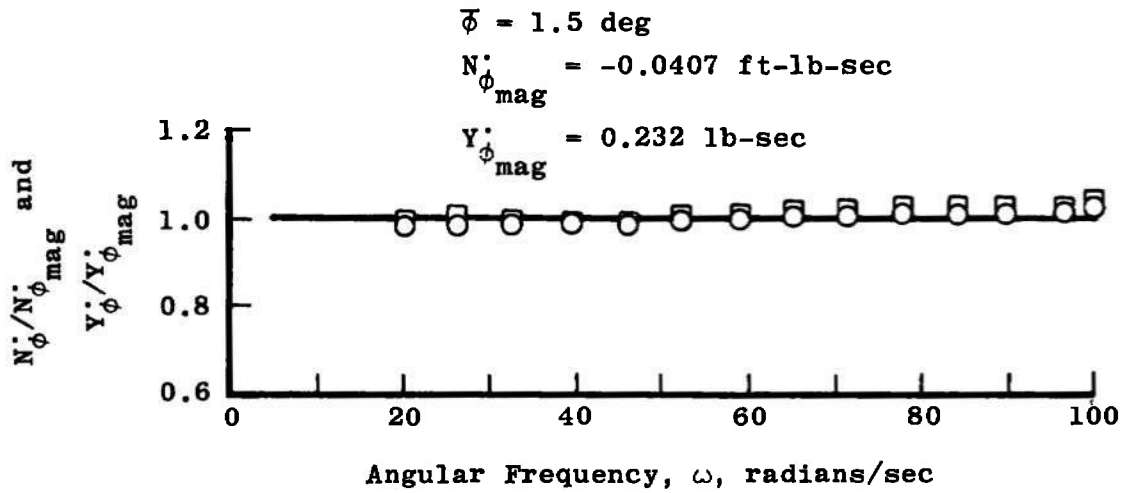

b. Variation with Frequency

Fig. 6 Comparison of Measured Yawing Moment and Side Force due to Roll Velocity to Magnetic Calibrator Input

Figure 6 shows the results obtained in measuring the yawing moment and side force due to roll velocity produced by the magnetic calibrator. Excellent agreement was obtained over a large range of yawing moment and side force due to roll velocity (Fig. 6a) and frequencies (Fig. 6b). The slight trend with frequency indicated in Fig. 6b is probably attributable to the uncertainty in obtaining the natural yaw frequency. These data indicate that the cross derivatives C_{Y_p} and C_{n_p} can be measured with this system; however, as shown in Section 3.1 and discussed in Section IV, model characteristics such as yaw natural frequency and products of inertia are very important in obtaining satisfactory data and must be considered in the model design.

The roll-damping characteristics obtained during the wind tunnel tests on the AGARD Model B are presented in Fig. 7. Only the $Re_{\infty, c} = 4 \times 10^6$ data are presented since no Reynolds number effects were found. The roll-damping coefficient, $C_{\ell_p} + C_{\ell_{\dot{\beta}}} \sin \alpha$, shows that the model is stable and that the data are symmetrical about $\alpha = 0$ for all Mach numbers, as would be expected. The magnitude of the damping decreases as $|\alpha|$ increases at $M_\infty = 2$ and 3, but the trend is reversed at $M_\infty = 4$. The magnitude of $C_{\ell_p} + C_{\ell_{\dot{\beta}}} \sin \alpha$ at $\alpha = 0$ decreases as Mach number increases, and the data are in good agreement with theoretical estimates obtained from Ref. 5. The static stability parameter, $C_{\ell_\beta} \sin \alpha$, is essentially zero at $\alpha = 0$, and the magnitude increases to produce more stability as $|\alpha|$ increases.

The static coefficients, C_N and C_m, are presented in Fig. 8 as a function of angle of attack, α. C_N increases linearly with α over the range tested, and the slope decreases as Mach number increases. C_m also increases with α, with the Mach 3 and 4 data being at practically the same level, whereas the Mach 2 data increase at a lesser rate. The data are in excellent agreement with data presented in Ref. 6.

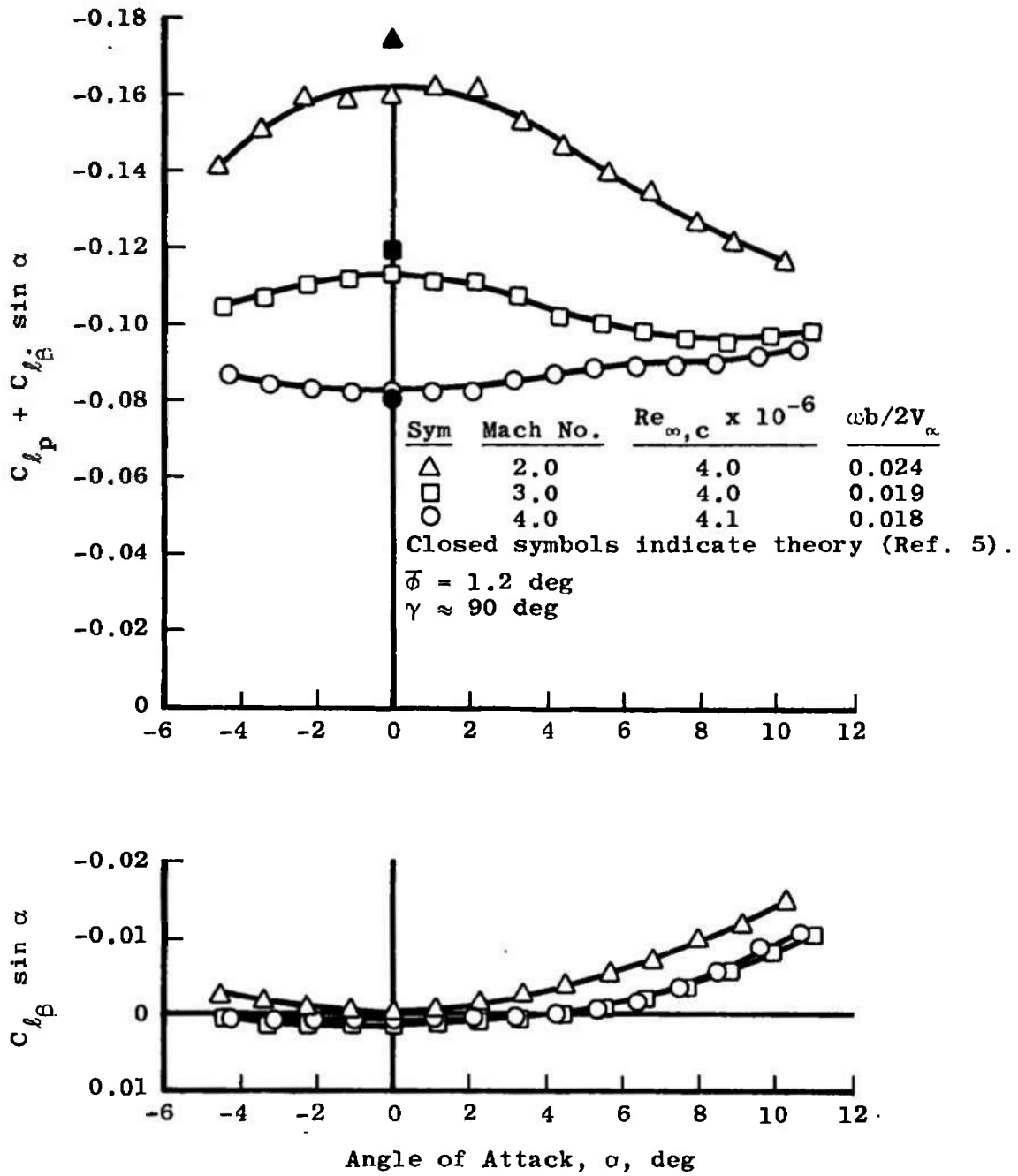

Fig. 7 Variation of Roll-Damping Coefficients with Angle of Attack and Mach Number

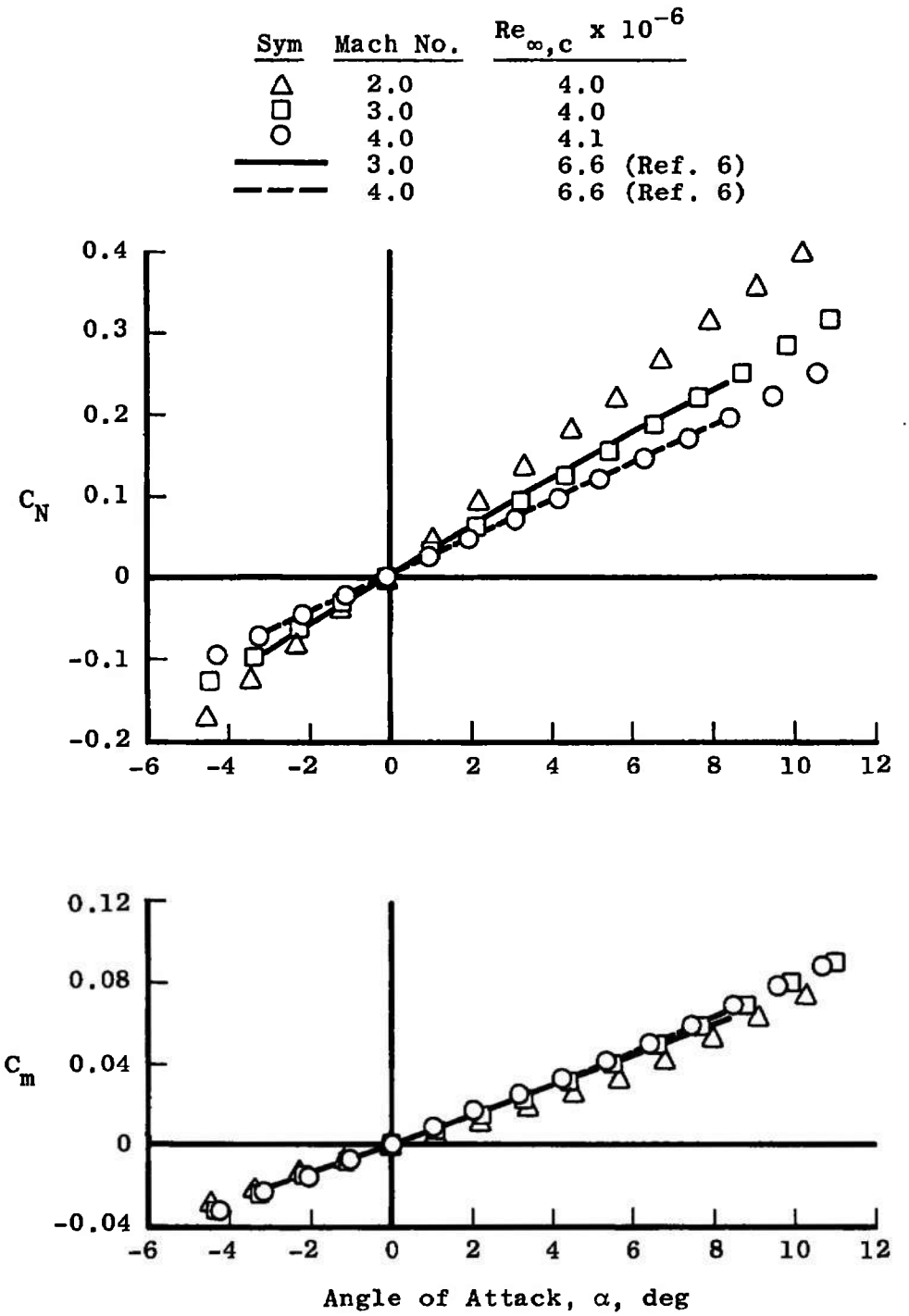

Fig. 8 Variation of Normal-Force and Pitching-Moment Coefficients with Angle of Attack and Mach Number

SECTION VI
CONCLUSIONS

A forced-oscillation, dynamic-stability test mechanism was developed for measuring the moments and forces due to roll velocity on lifting configurations. Bench tests and wind tunnel tests were conducted on an AGARD Model B to evaluate the mechanism. Conclusions based on the results of these tests are as follows:

1. The results of the bench tests indicated that the rolling moment, yawing moments, and side force due to roll velocity could be precisely measured by the mechanism.
2. The results of the wind tunnel tests indicated good agreement between the experimental and theoretical values of the roll-damping coefficient, $C_{\ell_p} + C_{\ell_{\dot{\beta}}} \sin \alpha$.
3. Yawing moment and side force due to roll velocity could not be obtained in these wind tunnel tests because of an adverse coupling of the roll and yaw natural frequencies and the large product of inertia, I_{xz}, of this particular model. By careful model design, it will be possible to obtain accurate values of the cross derivatives C_{Y_p} and C_{n_p}.

REFERENCES

1. Schueler, C. J., Ward, L. K., and Hodapp, A. E., Jr. "Techniques for Measurements of Dynamic Stability Derivatives in Ground Test Facilities." AGARDograph 121 (AD669227), October 1967.
2. Burt, G. E. "A Description of a Pitch/Yaw Dynamic-Stability, Forced-Oscillation Test Mechanism for Testing Lifting Configurations." AEDC-TR- (to be published).
3. Welsh, C. J. and Ward, L. K. "Structural Damping in Dynamic Stability Testing." AEDC-TR-59-5 (AD208776), February 1959.

4. Beers, Yardley. Introduction to the Theory of Error. Reading, Mass., Addison-Wesley Publishing Co., Inc., 1957, pp. 26-36.

5. Ribner, Herbert S. and Malvestuto, Frank S., Jr. "Stability Derivatives of Triangular Wings at Supersonic Speeds." NACA Report 908, 1948.

6. Coats, Jack D. "Force Tests of an AGARD Calibration Model B at M = 2.5 to 6.0." AEDC-TN-60-182 (AD244544), October 1960.

UNCLASSIFIED

Security Classification

DOCUMENT CONTROL DATA - R & D

(Security classification of title, body of abstract and indexing annotation must be entered when the overall report is classified)

1 ORIGINATING ACTIVITY (Corporate author)
Arnold Engineering Development Center
Arnold Air Force Station, Tennessee 37389

2a. REPORT SECURITY CLASSIFICATION
UNCLASSIFIED

2b GROUP
N/A

3 REPORT TITLE
A DESCRIPTION OF A FORCED-OSCILLATION TEST MECHANISM FOR MEASURING DYNAMIC-STABILITY DERIVATIVES IN ROLL

4 DESCRIPTIVE NOTES (Type of report and inclusive dates)
Final Report -- May 9, 1972

5 AUTHOR(S) (First name, middle initial, last name)
G. E. Burt, ARO, Inc.

6 REPORT DATE	7a. TOTAL NO OF PAGES	7b. NO OF REFS
June 1973	32	6

8a CONTRACT OR GRANT NO	9a. ORIGINATOR'S REPORT NUMBER(S)
b. PROJECT NO	AEDC-TR-73-49
c.	9b. OTHER REPORT NO(S) (Any other numbers that may be assigned this report)
d.	ARO-VKF-TR-72-211

10 DISTRIBUTION STATEMENT
Approved for public release; distribution unlimited.

11 SUPPLEMENTARY NOTES	12 SPONSORING MILITARY ACTIVITY
Available in DDC.	Aeronautical Systems Division (YHT), Wright-Patterson AFB, OH 45433

13 ABSTRACT A description is given of a forced-oscillation, dynamic-stability test mechanism for measuring the moments and forces due to roll velocity on lifting configurations. The mechanism can support models with a combined loading of up to 1200 pounds of normal force and 300 pounds of axial force and is water-cooled to permit testing in hypersonic tunnels. Bench tests were conducted using a magnetic calibrator, which indicated that the mechanism could precisely measure the rolling moment, yawing moment, and side force due to roll velocity. Wind tunnel tests were conducted on an AGARD Model B at Mach numbers of 2, 3, and 4 and at angles of attack from -4 to 11 deg to verify the design. Results of these tests indicated good agreement between the experimental and theoretical values of the roll-damping coefficient, but the cross derivatives (yawing moment and side force) due to roll velocity could not be obtained for this particular model because of an adverse coupling of the roll and yaw natural frequencies and a large product of inertia of the model.

DD FORM 1 NOV 65 1473

UNCLASSIFIED

Security Classification

14 KEY WORDS	LINK A		LINK B		LINK C	
	ROLE	WT	ROLE	WT	ROLE	WT
testing apparatus						
aerodynamic stability						
aerodynamic configurations						
supersonic wind tunnels						
damping						
moments of inertia						
roll						
yaw						